

Pseudoscalar Mediators: A WIMP model at the Neutrino Floor

Giorgio Arcadi^{1,*}, Manfred Lindner^{1,†}, Farinaldo S. Queiroz^{1,2,‡}, Werner Rodejohann^{1,§} and Stefan Vogl^{1,¶}

¹*Max-Planck-Institut für Kernphysik (MPIK),*

Saupfercheckweg 1, 69117 Heidelberg, Germany and

²*International Institute of Physics, Federal University of Rio Grande do Norte, Campus Universitário, Lagoa Nova, Natal-RN 59078-970, Brazil*

Due to its highly suppressed cross section (fermionic) dark matter interacting with the Standard Model via pseudoscalar mediators is expected to be essentially unobservable in direct detection experiments. We consider both a simplified model and a more realistic model based on an extended two Higgs doublet model and compute the leading one-loop contribution to the effective dark matter-nucleon interaction. This higher order correction dominates the scattering rate completely and can naturally, i.e. for couplings of order one, lead to a direct detection cross section in the vicinity of the neutrino floor. Taking the observed relic density and constraints from low-energy observables into account we analyze the direct detection prospects in detail and find regions of parameter space that are within reach of upcoming direct detection experiments such as XENONnT, LZ, and DARWIN.

* arcadi@mpi-hd.mpg.de

† lindner@mpi-hd.mpg.de

‡ queiroz@mpi-hd.mpg.de

§ werner.rodejohann@mpi-hd.mpg.de

¶ stefan.vogl@mpi-hd.mpg.de

INTRODUCTION

The presence of dark matter (DM) in our universe has been established in a variety of datasets [1] and the observations of the Planck satellite show that it accounts for 27% of the energy content of the Universe [2]. One of the most compelling dark matter candidates is a massive particles with weak-scale interactions, a so-called WIMP (Weakly Interacting Massive Particle) [3]. Thermal freeze-out of WIMPs furnishes a compelling solution for the DM puzzle since it correlates elegantly the DM relic density with the DM interaction strength with Standard Model (SM) particles via a single particle physics input, i.e. the thermally averaged pair annihilation cross section. In many scenarios this annihilation cross section is tied, by crossing symmetry, to the scattering cross section on nucleons; the experimentally favored value of the former frequently corresponds to a value of the latter that is in conflict with null results from direct DM searches [4–13]. This correlation can be weakened by considering next-to-minimal scenarios (see e.g. [14–16]) or models that lead to suppressed scattering rates due to the low energy scale in the process [17–27] such as the one investigated here.

The latter takes advantage of the different energy scales involved in the annihilation and scattering process to loosen the correlation. The scale for the annihilation cross section is set by the dark matter mass, whereas the momentum transfer in the dark matter-nucleon scattering is only $\mathcal{O}(100)$ keV. This can be exploited in the case of fermionic DM interacting via a light pseudoscalar field. As pointed out in [28, 29] the DM scattering cross section on nucleons at tree level is proportional to the fourth power of the momentum transfer and, therefore, the scattering rate in realistic direct detection experiments is essentially negligible (see however [18, 30]). The DM pair annihilation cross section, on the other hand, does not suffer from any suppression and the observed relic density can easily be generated by thermal freeze-out.

In the following, we investigate whether a non-negligible DM scattering rate can be generated at higher order in such a model and compute the DM nucleus scattering cross section. It turns out that for typical values of the involved couplings and masses, the loop-induced direct detection cross section takes values in the vicinity of the so-called “neutrino floor” [31], i.e. the cross section corresponding to the coherent scattering of neutrinos on nucleons. This process will induce a signal which is similar to the elastic scattering of a WIMP and thus represents an irreducible background [32–36]. Despite possibilities of discriminating signals from WIMP and neutrino scattering, for example by combining detectors with different target materials, the neutrino floor is customarily regarded as the ultimate sensitivity for future Direct Detection experiments such as XENONnT [37], LZ [38] and DARWIN [39].

The strength of a direct detection signal arising from high order corrections should be compared with existing constraints from low energy probes and collider searches to assess the importance of these loop effects in the WIMP-nucleon scattering. Throughout our analysis we assume that the entire dark matter relic density is determined by thermal freeze-out and do consider modification which could arise in non-standard cosmologies.

A reliable comparison between different observables requires going beyond a simplified setup. For this reason, we investigate the dark matter phenomenology in a simplified DM model as well as in a full UV-complete model [26, 40]. We show that the DM phenomenology of the simplified model differs from the full model due to the presence of new particles that cannot be fully decoupled.

The structure of this paper is as follows: First, we introduce a minimal simplified model for fermionic dark matter interacting with the SM via a pseudoscalar mediator. We discuss the phenomenology of the model with a particular emphasis on observables that are relevant for light pseudoscalars. In a second step, we generalize the simplified model and embed it in a gauge-invariant, UV-complete model. We investigate whether the conclusions derived in the simplified

model persist in the more general framework and comment on additional observables which become relevant in this case before concluding.

I. SIMPLIFIED MODEL

The model under consideration consists of a Dirac fermion χ ¹ which is a singlet under the SM gauge group and acts as our DM candidate. The interactions of χ with the SM are mediated by a s -channel pseudoscalar mediator a and can be described by the Lagrangian:

$$\mathcal{L} = ia \left(g_\chi \bar{\chi} \gamma_5 \chi + c_a \sum_f \frac{m_f}{v_h} \bar{f} \gamma_5 f \right), \quad (1)$$

where f is a SM fermion and $v_h = 246$ GeV the vacuum expectation value of the SM Higgs. We have assumed Yukawa-like couplings of the pseudoscalar with the SM fermions and parameterized our ignorance regarding the origin of this couplings by the rescaling parameter c_a (we will discuss a more concrete realization in the next section), while we have been agnostic concerning the DM coupling g_χ . The simplified model defined by this Lagrangian has only 4 free parameters, i.e. the masses m_χ and m_a of the new particles, the DM coupling g_χ and the rescaling parameter c_a .

As pointed out previously, the main goal of this work is to scrutinize potential direct detection prospects and we will focus our attention on the promising regions of parameter space. We consider masses of the pseudoscalar in the range $1 \leq m_a \leq 100$ GeV. The lower limit of the mass is chosen since it corresponds on the typical energy scales of nuclear processes. For masses of the mediator below this value, the conventional treatment of DM direct detection becomes questionable; we leave this to further study. As will be shown in the following, direct detection is irrelevant for $m_a \gtrsim 100$ GeV. Heavier mediator masses can be constrained by LHC searches for decays of a to SM fermions [25] while searches which target the invisible decay of a are currently not competitive [41, 42]. Since direct detection loses sensitivity for light dark matter we limit our study to $m_\chi \gtrsim 10$ GeV in what follows.

A. Dark Matter Annihilations and the Relic Density

Provided that the dark matter has been in thermal equilibrium with the SM plasma in the early Universe its present relic density is set by the abundance at freeze-out. Hence the dark matter density $\Omega_\chi h^2$ is determined by the thermally averaged pair annihilation cross section $\langle \sigma v \rangle$ of the DM. The observed value of $\Omega_\chi h^2 \simeq 0.12$ [2] is achieved for $\langle \sigma v \rangle \simeq 3 \times 10^{-26} \text{ cm}^3 \text{ s}^{-1}$. It receives contributions from annihilation processes of DM into SM fermions and, provided that the channel is kinematically open, aa pairs. Expanding $\langle \sigma v \rangle$ in velocity the leading contribution to the annihilation

¹ The case of Majorana DM is qualitatively the same but minor quantitative differences arise since DM is its own antiparticle in this case.

rate into SM fermions reads:

$$\begin{aligned} \langle \sigma v \rangle (\bar{\chi}\chi \rightarrow \bar{f}f) &\approx \sum_f \frac{2n_c^f c_a^2 m_\chi^2 g_\chi^2}{\pi(4m_\chi^2 - m_a^2)^2} \frac{m_f^2}{v_h^2} \\ &\approx \begin{cases} 7 \times 10^{-23} \text{ cm}^3 \text{ s}^{-1} g_\chi^2 c_a^2 \left(\frac{100 \text{ GeV}}{m_\chi}\right)^2 & m_a \ll m_t < m_\chi \\ 3 \times 10^{-26} \text{ cm}^3 \text{ s}^{-1} g_\chi^2 c_a^2 \left(\frac{100 \text{ GeV}}{m_\chi}\right)^2 & m_a \ll m_b < m_\chi < m_t \end{cases} \end{aligned} \quad (2)$$

Here the sum runs over the kinematically accessible SM fermions, m_f denotes their mass and n_c^f is their respective color factor. Due to the Yukawa-like coupling structure, the annihilation rate is dominated by the heaviest accessible fermion. In the parameter space of interest here this is either the bottom or the top quark. For convenience we also report two numerical estimates for the cases, $m_b < m_\chi < m_t$ and $m_\chi > m_t$. As can be seen, DM annihilations into top quarks are extremely efficient so that at least one of the couplings g_χ and c_a should be substantially smaller than 1 in order to comply with the DM relic density constraint. For $m_\chi < m_t$, in contrast, both g_χ and c_a need to be order one to achieve a viable thermal DM candidate.

The leading contribution to the other relevant annihilation cross section $\langle \sigma v \rangle (\chi\chi \rightarrow aa)$ only arises at $\mathcal{O}(v^2)$, i.e. it is p-wave suppressed. For $m_a \ll m_\chi$ it can be approximated as

$$\langle \sigma v \rangle (\bar{\chi}\chi \rightarrow aa) \approx \frac{g_\chi^4}{192\pi m_\chi^2} v^2 \approx 4.6 \times 10^{-25} \text{ cm}^3 \text{ s}^{-1} g_\chi^4 \left(\frac{100 \text{ GeV}}{m_\chi}\right)^2 \quad (3)$$

where we take $v \approx 0.3$ in the second step to give a reasonable estimate for the rate at freeze-out. In this regime the DM relic density can in principle be set by the annihilation cross section into aa pairs and the DM relic density and c_a could be very small since $\langle \sigma v \rangle (\bar{\chi}\chi \rightarrow aa)$ is only a function of m_χ and g_χ .

In order to relate the DM annihilation cross section with its relic density we have adopted the following relation [43]:

$$\Omega_\chi h^2 = 8.76 \times 10^{-11} \text{ GeV}^{-2} \left[\int_{T_f}^{T_0} g_*^{1/2} \langle \sigma v \rangle \frac{dT}{m_\chi} \right]^{-1} \quad (4)$$

where T_f and T_0 represent, respectively, the standard freeze-out and the present time temperature while $\langle \sigma v \rangle$ is the total cross, i.e. summed of all the kinematically accessible final states, DM annihilation cross section. This has been determined by numerically evaluating the integral:

$$\langle \sigma v \rangle = \frac{1}{8T m_\chi^4 K_2(m_\chi/T)} \int_{4m_\chi^2}^{\infty} ds \sqrt{s} (s - 4m_\chi^2) \sigma(s) K_1\left(\frac{\sqrt{s}}{T}\right) \quad (5)$$

where K_i denotes the Bessel function of i -th type. The velocity expansion presented above is only given for illustration, we do not use it in our computation.

The freeze-out temperature can be determined by numerically solving:

$$\sqrt{\frac{45}{\pi}} \frac{1}{M_{\text{Pl}}} \frac{45g_\chi}{4\pi^4} \frac{K_2(x)}{h_{\text{eff}}(T)} g_*^{1/2} m_\chi \langle \sigma v \rangle \delta(\delta + 2) = \frac{K_1(x)}{K_2(x)} - \frac{1}{x} \frac{d \log h_{\text{eff}}(T)}{d \log T}, \quad x = \frac{m_\chi}{T}, \delta = 1.5 \quad (6)$$

for $x_f = m_\chi/T$. h_{eff} represents the effective entropy degrees of freedom, g_χ are the internal degrees of freedom of the DM while $M_{\text{Pl}} \approx 1.22 \times 10^{19}$, GeV is the Planck mass. Our results have been double checked with the numerical package micrOMEGAs [44].

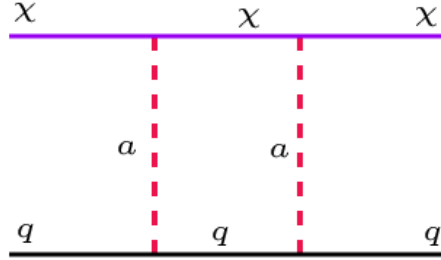


FIG. 1: Box diagram inducing the SI direct detection cross section in the simplified model.

Today the velocity of dark matter particles bound gravitationally in galaxies is limited by the escape velocity which implies $v = \mathcal{O}(10^{-3})$. Therefore, the rate of dark matter annihilations to pseudoscalar pairs $\langle\sigma v(\chi\chi \rightarrow aa)\rangle$ is completely negligible at present. In contrast, the rate for annihilation to $b\bar{b}$ final states is velocity independent and we expect that thermally produced dark matter has $\langle\sigma v\rangle = \mathcal{O}(10^{-26})\text{cm}^3\text{s}^{-1}$, see above. Gamma-ray observations in the direction of dwarf Spheroidal galaxies (dSphs) performed by the Fermi-LAT telescope provide strong constraints on $\langle\sigma v(\chi\chi \rightarrow b\bar{b})\rangle$ and essentially preclude this annihilation channel from dominating dark matter freeze-out for $m_\chi \lesssim 100\text{ GeV}$ [45, 46]. A complementary probe will be provided by the Cherenkov Telescope Array which has the potential to exclude the same annihilation cross section for masses above 200 GeV [47].

B. Direct Detection

In the scenario under consideration here the prospects for direct detection are generally considered to be rather poor since the effective interaction between a fermion DM candidate and nucleons generated by pseudoscalar exchange is suppressed by the momentum transfer, $\sigma \propto q^4$. Moreover, the cross section is spin-dependent. The direct detection phenomenology has been studied in detail for example in [18, 19, 30].

The goal of this work is to reconsider direct detection including higher-order effects. In particular, box diagrams with one SM quark and two pseudoscalar states [28, 48] running in the loop generate a Spin-Independent (SI) interaction, see Fig. 1 for a representative diagram. Despite its origin at higher order, the scattering rate induced by this SI interaction is not necessarily suppressed with respect to the one originating from the tree level pseudoscalar exchange since there is no momentum suppression. On the contrary, an A^2 enhancement due to the coherent character of SI interactions increases the experimental sensitivity even further.

The scattering amplitude can be computed starting from the following effective Lagrangian [49]:

$$\mathcal{L} = g_\chi^2 c_a^2 \sum_q \frac{m_q^2}{v_h^2} (C_{V,q} \bar{\chi} \gamma^\mu \chi \bar{q} \gamma_\mu q + C_{S,q} \bar{\chi} \chi \bar{q} q). \quad (7)$$

where q is a SM quark and the sum runs over all quark species.

The coupling of a to the light quarks is highly suppressed due to the SM Yukawa-like coupling structure and, therefore, the only sizable contribution to the direct detection rate is expected from

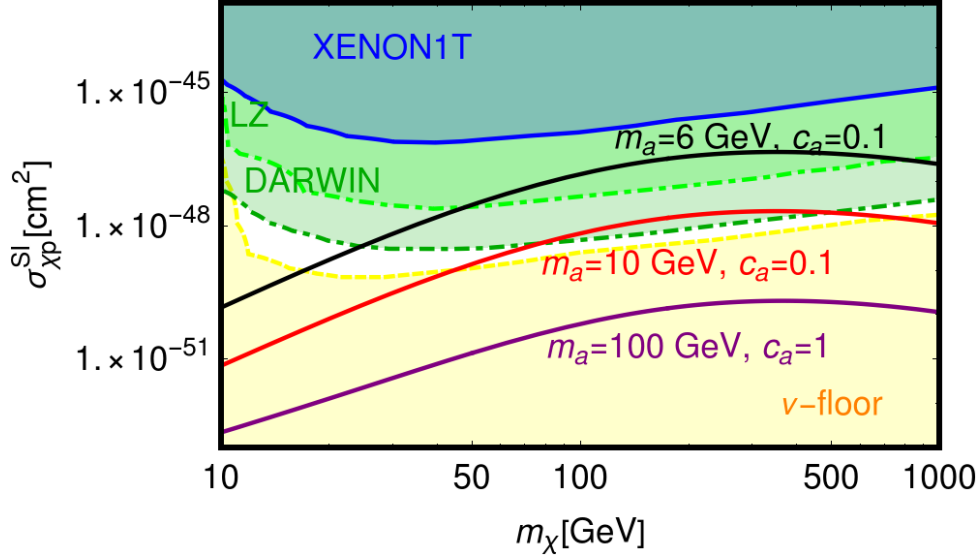


FIG. 2: SI cross section induced at one-loop as function of the DM mass m_χ , for $g_\chi = 0.5$ and for four assignments of (m_a, c_a) , as reported on the plot. The blue region is currently excluded by XENON1T. The light green (dark green) region will be probed by LZ (DARWIN). The yellow region corresponds to the sensitivity to coherent scattering processes of neutrinos on nucleons.

the heavy quarks. This allows for an instant simplification since only valence quarks contribute to the nuclear expectation value of the vector current and we can drop the vector piece in the effective Lagrangian right away. The contribution from the scalar piece is more subtle. Top, bottom and charm quark are clearly heavier than the proton and should be integrated out of an effective theory that describes physics at the nuclear scale. This can be done by invoking the relation between the heavy quark content of the nucleus and the gluon condensate given by [50]

$$m_Q Q\bar{Q} = -\frac{\alpha_s}{12\pi} G_{\mu\nu} G^{\mu\nu}, \quad (8)$$

where α_s is the strong coupling constant and $G_{\mu\nu}$ denotes the field strength tensor of QCD. The numerical value for the gluon condensate is given by $\alpha_s \langle n | G_{\mu\nu} G^{\mu\nu} | n \rangle = -\frac{8}{9} m_N f_{TG}$ with $f_{TG} \approx 0.894$, see [51] for a detailed discussion of how f_{TG} is extracted from low energy data².

The corresponding SI cross section (for definiteness we will consider the case of scattering on protons) can be schematically expressed as:

$$\sigma_{\chi p}^{\text{SI}} = \frac{\mu_\chi^2}{\pi} c_a^4 g_\chi^4 |F_l(m_\chi, m_a)|^2, \quad (9)$$

² We adopt the default value used by micrOMEGAs [44].

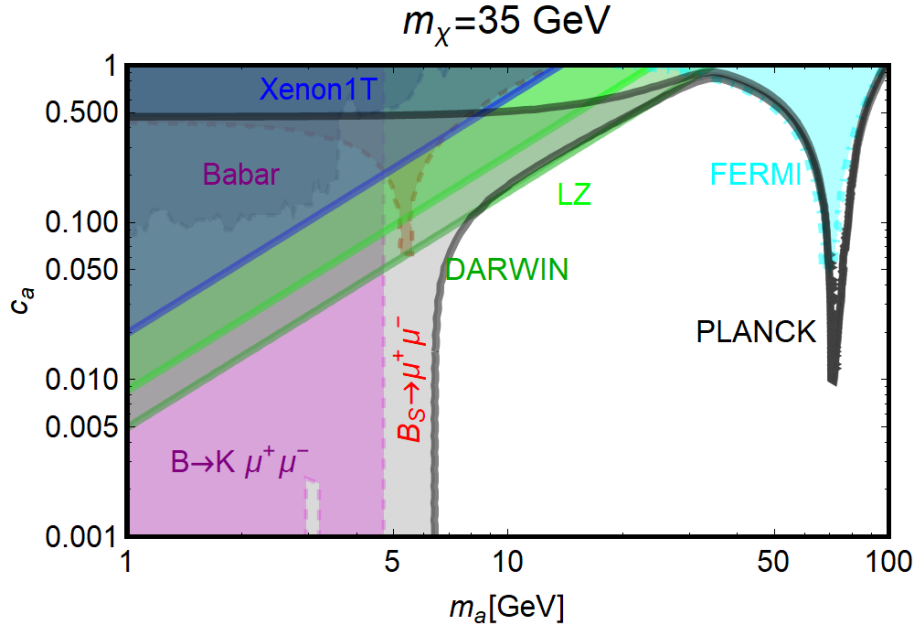


FIG. 3: Comparison of various constrains and direct detection prospects in the $m_a - c_a$ plane for $m_\chi = 35 \text{ GeV}$ and $g_\chi = 0.5$. The direct detection limit from XENON1T is shown in blue while the prospects for LZ (DARWIN) are shown in light (dark) green. Indirect detection limits exclude the cyan region while the relic density constraint can be fulfilled in the gray band. The bounds from BaBar are depicted in purple whereas $B \rightarrow K \mu^+ \mu^-$ is shown in magenta and $B_s \rightarrow \mu^+ \mu^-$ in red.

where μ_χ is the reduced mass while:

$$F_l(m_\chi, m_a) = \frac{2}{27} f_{TG} \sum_q \frac{m_q m_p}{v_h^2} C_{S,q}. \quad (10)$$

The expression for $C_{S,q}$ is rather lengthy and we do not report it here but refer the reader to App. A instead.

Two comments about the reliability of this result are in order. First, the simplified model in which this computation has been made is not gauge invariant. Generically we expect that an UV-completion of the simplified model will introduce new degrees of freedom to restore gauge-invariance. These new fields could allow for additional diagrams and therefore the amplitude considered here cannot be expected to be the full result. We will comment on this in more detail in Sec. II where we analyze a representative example of such an UV-completion. In addition, there is a further complication which is related to the relation we employed to replace the heavy quarks with the gluons in Eq. (8). This procedure is justified if the loop that generates the four-fermion interaction and the loop that relates the quarks to the gluon-condensate factorize. While this assumption is reasonable for heavy new physics which can be integrated out at energies above the top mass, it is not fully appropriate in the scenario under scrutiny here since we are interested in $m_a < m_t$. In this case, the correct top mass dependence of the effective dark matter gluon interaction is only

recovered by a two-loop computation of the effective dark matter gluon interaction [52] which is beyond the scope of this work. In the following, we will rely on Eq. (8) while keeping in mind that the result is only approximate.

The behavior of the scattering cross section, as a function of the DM mass, for $g_\chi = 0.5$ and for some different assignments of c_a and m_a , is reported in Fig. 2. The predictions of the scattering cross sections are compared with the current exclusion limit, as set by XENON1T [12], and the projected sensitivities of future experiments, i.e. LZ and DARWIN. The plot also reports the so-called “neutrino floor” [31], which corresponds to the sensitivity of direct detection experiments to coherent scatterings of neutrinos with nuclei.

C. Constraints from low energy observables

A light pseudoscalar field, $m_a \lesssim 10$ GeV can influence a broad variety of low energy observables. For example, it can lead to sizable enhancements of the decay rates of K and B mesons either due to tree-level a exchange or due to the loop induced flavor changing neutral current (FCNC) $b \rightarrow sa$ and $s \rightarrow da$ transitions [53, 54]. This can change the branching ratios of the aforementioned mesons into lighter mesons and/or leptons. These limit will be most stringent for light pseudoscalar masses, i.e. below the masses of the B and/or K mesons, when a can be produced on-shell in the decay processes. An extensive list of constraints on light pseudoscalars has been presented e.g. in [19]. Since we are only interested in $m_a > 1$ GeV we will focus on three of those processes $\Upsilon \rightarrow a\gamma$, $B_s \rightarrow \mu^+\mu^-$ and $B \rightarrow K\mu^+\mu^-$.

The first process is the radiative tree-level decay $\Upsilon \rightarrow \gamma a$ followed by the subsequent decay of a to SM particles. Searches for these decays have been performed by the BaBar collaboration [55–57]. Depending on the mass of a hadronic decays or the leptonic final states $\tau^+\tau^-$ and $\mu^+\mu^-$ pose the strongest constraints on the model. In the following we merge these bounds into a single limit which we label BaBar for simplicity.

The branching fraction for the next process, $B_s \rightarrow \mu^+\mu^-$, has been measured jointly by the CMS and LHCb collaboration [58] to be $Br(B_s \rightarrow \mu^+\mu^-)^{exp} = (2.8_{-0.6}^{+0.7}) \times 10^{-8}$. The experimental value can be related to the theoretical prediction by:

$$Br(B_s \rightarrow \mu^+\mu^-)^{exp} \approx \frac{1}{1 - y_s} Br(B_s \rightarrow \mu^+\mu^-)^{th} \quad (11)$$

where the parameter $y_s = \frac{\Delta\Gamma_{B_s}}{2\Gamma_{B_s}} = 0.061$ [59] accounts for the effect of $B_s - \bar{B}_s$ oscillations. The theoretical prediction of $Br(B_s \rightarrow \mu^+\mu^-)$ is given by:

$$Br(B_s \rightarrow \mu^+\mu^-)^{th} = \tau_{B_s} \frac{\alpha^2 G_F^2 m_{B_s}}{16\pi^3} \sqrt{1 - \frac{4m_\mu^2}{m_{B_s}^2}} |V_{tb}V_{ts}|^2 f_{B_s}^2 m_\mu^2 \\ \times |C_{10}^{SM} + \frac{m_{B_s}^2}{2m_\mu(m_b + m_s)} \frac{m_t^2}{(m_{B_s}^2 - m_a^2)} C_{P,a}|^2, \quad (12)$$

where G_F is the Fermi constant, V_{ij} are entries of the CKM matrix. Here f_{B_s} is the B_s -meson decay constant while τ_{B_s} and m_{B_s} denote the lifetime and mass, respectively. The SM contribution to the effective operator expansion defined for example in [60] (see also [61, 62]) is $C_{10}^{SM} \simeq -4.103$.

In the simplified model determining $C_{P,a}$ poses a problem since a direct computation shows that the amplitude is divergent. This behavior is not surprising given that the model is not UV-complete.

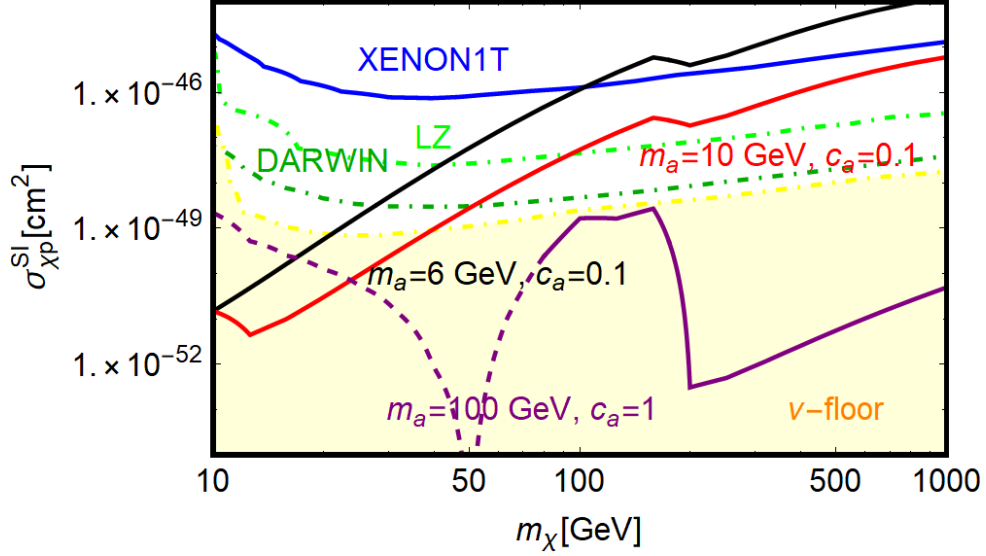


FIG. 4: Contours of the correct DM relic density, in the plane $(m_\chi, \sigma_{\chi p}^{\text{SI}})$ for three benchmark assignments of (m_a, c_a) . The dashed parts of the contours are excluded by indirect detection while the solid parts comply with all constraints. The dot-dashed light (dark) green line corresponds to the projected sensitivity of LZ (DARWIN). The yellow shaded region is below the so called “neutrino floor”.

In order to get an estimate for the coefficient $C_{P,a}$ we follow the reasoning proposed in [19] and replace the divergence by a cut-off of the form $\log(\Lambda^2/m_t^2)$, where Λ should be interpreted as the scale at which the UV-completion of the simplified model cures the divergence. Under these assumption one expects

$$C_{P,a} \approx \frac{c_a^4}{8 \sin^2 \theta_W} \log \left(\frac{\Lambda^2}{m_t^2} \right). \quad (13)$$

For illustration we adopt the assignment $\Lambda = 1 \text{ TeV}$. We would like to highlight that a proper assessment of the limit from this kind of flavor violating processes cannot be achieved within a simplified setup. This issue does not subsist in a gauge UV-complete setup and we will discuss a more robust bound in the next section, where a gauge invariant model will be discussed.

Finally, we consider the constraint arising from the $B \rightarrow K \mu^+ \mu^-$. Its branching fraction is given by (for simplicity we omit the SM contribution):

$$\begin{aligned} Br(B \rightarrow K \mu^+ \mu^-) &= \tau_B \frac{\alpha^2 G_F^2}{512 \pi^5 m_B^3} |f_0(m_a^2)|^2 m_\mu^2 m_b^2 \sqrt{\lambda(m_B^2, m_K^2, m_a^2)} \\ &\times \frac{m_t^4}{m_W^4} \left(\frac{m_B^2 - m_K^2}{m_b - m_s} \right)^2 |C_{P,a}|^2 \sqrt{1 - \frac{4m_\mu^2}{m_a^2}}, \end{aligned} \quad (14)$$

where $\lambda(a, b, c) = (a - b - c)^2 - 4bc$ while f_0 is a QCD form factor whose most recent numerical determination can be found in [63, 64]. Similar to the case of $B_s \rightarrow \mu^+ \mu^-$ a well-defined assessment

of the experimental constraint requires a UV complete realization but we will again provide an illustrative estimate by taking $\Lambda = 1 \text{ TeV}$ and compare it with the outcome of the experimental search by LHCb [65]. This comparison is actually less trivial with respect to the case of $B_s \rightarrow \mu^+ \mu^-$. Indeed the observable adopted for experimental analyses is actually $dBr(B \rightarrow K \mu^+ \mu^-)/dq^2$ where q^2 is the squared invariant mass of the final state muons, rather than the total branching ratio. In order to assess the limit we have imposed that the sum of the SM contribution, which is obtained by integrating dBr/dq^2 (the corresponding expression is found, for example, in [60]) over the width of the bin, and NP contribution, as given by eq. 14, does not exceed the observed limit in each of the q^2 bins of [65] (the NP contribution is more relevant when a decays on shell into a muon pair, i.e. for $q^2 = m_a^2$).

D. Results and Discussions

We can now confront direct and indirect detection with low-energy observables and investigate to which extent the loop-induced SI interactions can probe thermal DM. To have an idea of the relative constraining power of the different observables we first show the constraints in the m_a, c_a plane in Fig. 3. We have fixed $m_\chi = 35 \text{ GeV}$ and $g_\chi = 0.5$ since these parameters do not have an impact on the meson decays.

As can be seen all limits from meson decays become irrelevant for $m_a \gtrsim 5 \text{ GeV}$ with the exception of the one from $B_s \rightarrow \mu^+ \mu^-$. This constraint remains competitive with the limit from XENON1T even at higher masses. Next generation experiments provide a better sensitivity; however they can only moderately improve the constraints on c_a because of the very strong dependence, as c_a^4 , of the scattering cross section.

The behavior of the relic density band can be understood as follows: For low m_a the full relic density can be explained from $\chi\chi \rightarrow aa$ annihilations alone and c_a has to be smaller than ~ 0.5 in order to avoid overproduction. As $\langle\sigma v(\chi\chi \rightarrow aa)\rangle$ decreases with increasing m_a an additional contribution from $b\bar{b}$ final states becomes necessary to produce the correct relic density and c_a is confined to a band. Finally, once annihilations into pseudoscalars cease to be efficient, $b\bar{b}$ remains the only open channel and the allowed range of c_a is constrained to a band that is smaller than the line width in our plot. As expected the annihilation rate features a resonant enhancement when $m_a \approx 2m_\chi$.

The Fermi-LAT sensitivity³ is only sufficient to constraint the region where $\chi\chi \rightarrow b\bar{b}$ is the dominant annihilation channel and, therefore, its reach is limited to the resonance region here. In the future direct detection searches can probe thermal DM for $m_a \lesssim 20 \text{ GeV}$ but for $m_a \lesssim 5 \text{ GeV}$ the limit from $B_s \rightarrow \mu^+ \mu^-$ forces c_a to be so small that no detection can be expected.

With Fig. 3 in mind we can now make an educated guess and select three promising benchmark points (BM1 with $m_a = 6 \text{ GeV}$, $c_a = 0.1$, BM2 with $m_a = 10 \text{ GeV}$, $c_a = 0.1$ and BM3 with $m_a = 100 \text{ GeV}$, $c_a = 1$) for which we analyze the direct detection prospects in more detail. The points are allowed by low energy observables and allow for a successful generation of thermal dark matter. By requiring a thermal dark matter candidate one of the two remaining parameters can be fixed and we can derive the thermal value for $\sigma_{\chi p}^{SI}$ as a function of m_χ , see Fig. 4.

³ The Fermi-LAT exclusion limit, in Fig. 3 and elsewhere in this work has been determined by imposing that the DM annihilation cross section into $b\bar{b}$ final states, in the $v \rightarrow 0$ limit, is lower than the limit reported in [45] for this annihilation channel. This procedure is reliable since, given the Yukawa-like couplings of the pseudoscalar mediator the $b\bar{b}$ is the only relevant SM annihilation final state as long as $m_b < m_\chi < m_t$ (Note however, that hypothetical black hole physics could lead to a dark matter density spike and substantially improving the experimental sensitivity [66]). For $m_\chi > m_t$ DM annihilations are dominated by the $t\bar{t}$ final state but this is not problematic since indirect detection cannot yet probe the WIMP paradigm at this high DM masses.

The shape of the contours can be understood as follows. For the two benchmarks with light m_a and $c_a = 0.1$ the DM relic density is mostly determined by the $\bar{\chi}\chi \rightarrow aa$ process. In this case the correct relic density can be described by a simple relation between g_χ and m_χ , $g_\chi^2 \approx 0.6 m_\chi / (100 \text{ GeV})$ [19]. This implies that the predicted scattering cross section increases with the DM mass. The small bumps at $m_\chi \simeq 200 \text{ GeV}$ are induced by a non-negligible contribution from the $t\bar{t}$ final state to the DM annihilation cross section. In the case of the benchmark with $c_a = 1$, $m_a = 100 \text{ GeV}$ the relic density is mostly determined by the annihilation into fermion pairs instead. As a consequence we notice two sharp drops in the predicted cross section which are due to the s -channel pole, $m_\chi \sim m_a/2$ and to the opening of the $t\bar{t}$ final state.

As can be seen, the DM scattering cross section of a thermal WIMP is clearly in reach of the next generation of direct detection facilities for small values of m_a , even for $c_a = 0.1$ provided $m_\chi \gtrsim 50 \text{ GeV}$. In contrast, for $m_a = 100 \text{ GeV}$ and $c_a = 1$, the predicted cross section lies almost entirely within the “neutrino floor”. This last benchmark is particularly interesting since it demonstrates the existence of a thermal DM model with a direct detection rate that is naturally, i.e. for $\mathcal{O}(1)$ couplings, below the sensitivity of present and proposed direct detection experiments.

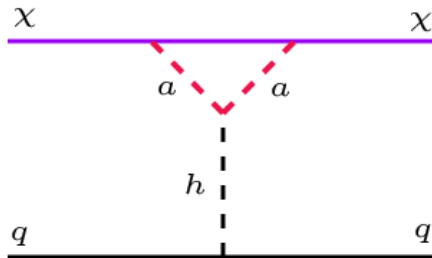


FIG. 5: Additional diagram contributing of the DM SI cross section if the pseudoscalar mediator couples to the SM Higgs.

II. GAUGE INVARIANT REALIZATION

We will now investigate whether the interesting features of the simplified model described above persist in theoretically consistent realizations which respect gauge invariance. One possibility to induce a coupling of the form $a\bar{f}\gamma_5 f$ between a SM singlet pseudoscalar a and the SM fermions is to mix it with a second pseudoscalar state A which belongs to a Two Higgs Doublet Model (2HDM) extension of the SM [26, 48, 67] (see [68, 69] for work focusing on mixing between the CP-even scalars). The scalar potential of such a model is given by

$$V = V_{\text{2HDM}} + \frac{1}{2}m_{a_0}a_0^2 + \frac{\lambda_a}{4}a_0^4 + \left(i\kappa a_0 H_1^\dagger H_2 + \text{h.c.}\right), \quad (15)$$

where V_{2HDM} denotes the usual potential of a 2HDM [70], H_1 and H_2 are two scalar $SU(2)$ doublets while κ denotes the coupling between the doublets and the pseudoscalar a_0 . In the following κ is assumed to be real.

Just as in the simplified model the field a_0 is coupled to the DM χ as:

$$\mathcal{L} = ig_\chi a_0 \bar{\chi} i\gamma^5 \chi. \quad (16)$$

After EW symmetry breaking the scalar sector of the theory is composed by four CP-even scalars h, H, H^\pm , and two CP-odd states. The two pseudoscalars mix and we introduce the fields a, A defined by

$$\begin{pmatrix} A_0 \\ a_0 \end{pmatrix} = \begin{pmatrix} \cos \theta & -\sin \theta \\ \sin \theta & \cos \theta \end{pmatrix} \begin{pmatrix} A \\ a \end{pmatrix} \quad (17)$$

with the mixing angle θ given by

$$\tan 2\theta = \frac{2\kappa v_h}{m_{A_0}^2 - m_{a_0}^2}. \quad (18)$$

Omitting the kinetic terms and the interactions with gauge bosons for simplicity, the interaction Lagrangian in the mass basis reads

$$\mathcal{L} = \mathcal{L}_{\text{DM}} + \mathcal{L}_{\text{scalar}} + \mathcal{L}_{\text{Yuk}} \quad (19)$$

where \mathcal{L}_{DM} is the DM Lagrangian:

$$\mathcal{L}_{\text{DM}} = g_\chi (\cos \theta a + \sin \theta A) \bar{\chi} i \gamma_5 \chi. \quad (20)$$

$\mathcal{L}_{\text{scalar}}$ contains the trilinear interactions between the (pseudo)scalar fields

$$\mathcal{L}_{\text{scalar}} = \frac{1}{2v_h} (m_A^2 - m_a^2) [\sin 4\theta a A + \sin^2 2\theta (A^2 - a^2)] (\sin(\beta - \alpha)h + \cos(\beta - \alpha)H), \quad (21)$$

while \mathcal{L}_{Yuk} contains the Yukawa interactions with fermions

$$\mathcal{L}_{\text{Yuk}} = \sum_f \frac{m_f}{v_h} (\xi_f^h h \bar{f} f + \xi_f^H H \bar{f} f - i\xi_f^A A \bar{f} \gamma_5 f - i\xi_f^a a \bar{f} \gamma_5 f). \quad (22)$$

The parameters ξ_f^ϕ with $\phi = h, H, A, a$ depend on the angles α, β (as well as θ for A, a) according to the couplings of the original $H_{1,2}$ doublets with the SM fermions. For definiteness, we will consider the type-II 2HDM. Furthermore, we will assume the so-called alignment limit, i.e. $\beta - \alpha = \frac{\pi}{2}$, which ensures that the interactions of h are similar to those of the SM-Higgs. Under these assumptions the scaling factors of the Yukawa couplings are:

$$\begin{aligned} \xi_f^h &= 1, \\ \xi_u^H &= \frac{1}{\tan \beta}, \quad \xi_d^H = \xi_e^H = \tan \beta, \\ \xi_u^A &= \frac{\cos \theta}{\tan \beta}, \quad \xi_d^A = \xi_e^A = \cos \theta \tan \beta, \\ \xi_u^a &= -\frac{\sin \theta}{\tan \beta}, \quad \xi_d^a = \xi_e^a = -\sin \theta \tan \beta. \end{aligned} \quad (23)$$

As a final simplification we will assume a degenerate spectrum for the scalars and take $m_H = m_A = m_{H^\pm}$. The simplified model discussed previously is recovered in the limit $m_\chi, m_a \ll m_A, m_H, m_{H^\pm}, \theta \ll 1$ and $\tan \beta = 1$. However, it should be kept in mind that the heavy Higgs sector cannot be removed completely. For a given value of θ , m_A cannot be arbitrarily larger than

m_a ; otherwise violation of unitarity would be encountered in aa, aA and AA scattering into gauge bosons. The unitarity condition is given by [40]:

$$|\Lambda_{\pm}| \leq 8\pi, \text{ where } \Lambda_{\pm} = \left[\frac{\Delta_H^2}{v_h^2} - \frac{\Delta_a^2(1 - \cos 4\theta)}{8v_h^2} \pm \sqrt{\frac{\Delta_H^2}{v_h^2} + \frac{\Delta_a^4(1 - \cos 4\theta)}{8v_h^4}} \right]$$

with $\Delta_a = m_A^2 - m_a^2$, and $\Delta_H = M^2 - m_{H\pm}^2 + 2m_W^2 - m_h^2/2$. (24)

In the limit $M = m_A = m_{H\pm} \gg m_a$ and taking maximal mixing, i.e. $\sin 2\theta = 1$, this leads to an upper limit on m_A of about 1400 GeV which can be weakened by lowering the value of $\sin \theta$.

The upper limit on the scalar masses should be compared to the lower bounds on the 2HDM from collider searches [71–74] and precision observables [70, 75]. Furthermore, as will be discussed in more detail in the next subsection, the heavy Higgs bosons contribute substantially to meson decays. In particular the observed branching ratios of weak radiative B-meson decay impose a lower bound of approximately 570 GeV [76] on $m_{H\pm}$ which depends only weakly on $\tan \beta$. In addition, searches for the production of a in association with Z and h constrain parts of the parameter space [26, 67].

Finally, for $m_a \leq m_h/2$, the coupling between the light pseudoscalar a and the SM like-Higgs leads to exotic decays of the SM Higgs bosons. The rate for $h \rightarrow aa$ is given by [48]:

$$\Gamma = \frac{(m_A^2 - m_a^2)^2}{32\pi m_h v_h} \sin^4 2\theta \sqrt{1 - \frac{4m_a^2}{m_h^2}}, \quad (25)$$

The pseudoscalar can either decay into SM fermions or into a pair of DM states. At the moment the most effective searches have been performed by CMS [77] and rely on the $2b2\mu, 4\tau$ and 4μ final states. However, these searches are restricted to specific ranges of m_a . In addition, the experimental determination of the Higgs signal strength $\mu \simeq 1.09 \pm 0.11$ [78] provides an independent constraint of the total width of h into non-standard decay channels.

In the following we will analyze the phenomenology of the gauge invariant model and comment on the differences compared to the simplified model.

A. Dark Matter Annihilations and the Relic Density

Due to the mixing between the two pseudoscalars a and A , the DM annihilations into SM fermions are induced by two mediators. As long as $m_\chi \ll m_A/2$ and $m_\chi < (m_h + m_a)/2$, the DM relic density is controlled by the same processes as in the simplified model. The expression provided in the previous section remain valid provided that the rescaling $c_a \rightarrow \cos \theta \xi_f^a, f = u, d, e$ is used; similarly the rate for the annihilation into aa final state should be rescaled by a factor $\cos^2 \theta$.

When $m_\chi \sim m_A/2$ the DM annihilation cross section is enhanced, with respect to the simplified case, by an additional s -channel resonance. Furthermore, as the DM mass increases, new annihilation channels become accessible, namely ha, hZ, hA, aA and AA (the latter two give a suppressed contribution, with respect to the aa , since their rates depend on greater powers of $\sin \theta$).

The main difference, concerning the DM relic density between the full and the simplified model, will originate from the $\tan \beta$ dependence of the coupling of the pseudoscalar field with the SM fermions, encoded in the parameters ξ_f^a .

B. Direct Detection

In the case of direct detection, the changes are more striking. As expected, the new fields and interactions introduced in the gauge invariant realization of the pseudoscalar mediator model contribute at the same order as the light pseudoscalar itself and generate additional diagrams. The interaction between a and the Standard Model Higgs h allows for an effective dark-matter-Higgs coupling which is generated by a triangle diagram with pseudoscalars in the loop, see Fig. 5. This generates a new contribution to SI cross section. The triangle contribution to the scalar operator reads [48]:

$$\mathcal{L} = \tilde{C}_S \bar{\chi} \chi \bar{q} q, \quad \tilde{C}_S = \frac{g_\chi^2 \sin^2 2\theta}{32\pi^2 m_h^2} \frac{m_A^2 - m_a^2}{m_a^2} \frac{m_\chi m_q}{v_h^2} G\left(\frac{m_\chi^2}{m_a^2}\right) \bar{\chi} \chi \bar{q} q, \quad (26)$$

where the loop function $G(x)$ is given by

$$G(x) = \frac{1}{2x^2} ((x-1) \log(x) - 2x) + \frac{(3x-1)}{2x^2 \sqrt{4x-1}} \left[\log\left(\frac{-1+2x-i\sqrt{-1+4x}}{2x}\right) + \log\left(\frac{-1+4x-2x^2-i(-1+2x)\sqrt{-1+4x}}{2x^2}\right) \right]. \quad (27)$$

The new contribution to the scalar coefficient \tilde{C}_S depends on additional parameters of the theory, i.e. m_h and m_A , and, consequently, the relative importance of the box and the triangle diagram is model dependent. However, the unitarity constraints in the scalar sector ensure that the ratio m_A/m_h can not exceed values of $\mathcal{O}(1)$ unless $\sin\theta$ becomes small. In addition, also diagrams with H or A are generated but the larger mass of the heavy scalars suppresses their contribution sufficiently to make them irrelevant for the light m_a scenario under consideration here.

The scalar coefficient for the interaction with the heavy quarks can be related to the coupling with gluons using Eq. (8) and for the full contribution we sum the box and the triangle induced contributions.⁴

C. Constraints from low energy Observables

As discussed in the previous section, constraints from flavor violating decays of the B -mesons cannot be applied easily in a simplified model. In this model, in contrast, it is possible to properly determine the EFT coefficients contributing to their decay rates. The results for $Br(B_s \rightarrow \mu^+ \mu^-)$ in the general 2HDM can be written as [60, 62]

$$Br(B_s \rightarrow \mu^+ \mu^-)^{th} = \tau_{B_s} \frac{\alpha^2 G_F^2 m_{B_s}}{16\pi^3} \sqrt{1 - \frac{4m_\mu^2}{m_{B_s}^2}} |V_{tb} V_{ts}|^2 f_{B_s}^2 m_\mu^2 \times \left[\left| C_{10} + \frac{m_{B_s}^2 C_P}{2m_\mu(m_b + m_s)} \right|^2 + |C_S|^2 \frac{m_{B_s}^2 (m_{B_s}^2 - 4m_\mu^2)}{4m_\mu^2 (m_b + m_s)^2} \right]. \quad (28)$$

⁴ Since the momentum flow through the Higgs propagator is negligible the two triangle loops can always be factorized and, in contrast to the box diagram, no subtleties regarding Eq. (8) arise.

The additional EFT coefficient has to be introduced since all the new scalars contribute non-negligibly to the decay process. For simplicity we report only the effective coefficient associated with the light pseudoscalar field:

$$|C_{P,a}|^2 = \frac{m_W^4 \sin^4 \theta}{(m_{B_s}^2 - m_a^2)^2 + m_a^2 \Gamma_a^2} |F_P(x_t, x_b, x_\mu, x_{H^\pm})|^2,$$

with

$$F_P(x_t, x_b, x_\mu, x_{H^\pm}) = -\frac{\sqrt{x_b x_\mu x_t} \xi_l}{2 \sin^2 \theta_W} \left\{ \frac{\xi_u^3 x_t}{2} \left[\frac{1}{x_{H^\pm} - x_t} - \frac{x_H^\pm}{(x_{H^\pm} - x_t)^2} \log \left(\frac{x_{H^\pm}}{x_t} \right) \right] \right. \\ \left. + \frac{\xi_u}{4} \left[-\frac{3x_{H^\pm} x_t - 6x_{H^\pm} - 2x_t^2 + 5x_t}{(x_t - 1)(x_{H^\pm} - x_t)} + \frac{x_{H^\pm} (x_{H^\pm}^2 - 7x_{H^\pm} + 6x_t)}{(x_{H^\pm} - x_t)^2 (x_{H^\pm} - 1)} \log x_{H^\pm} \right. \right. \\ \left. \left. - \frac{x_{H^\pm} (x_t^2 - 2x_t + 4) + 3x_t^2 (2x_t - 2x_{H^\pm} - 1)}{(x_{H^\pm} - x_t)^2 (x_t - 1)^2} \log x_t \right] \right\}, \quad (29)$$

where $x_i = m_i^2/m_W^2$, $i = \mu, b, t, H^\pm$ ⁵. For the explicit expressions of the other coefficients generated in the 2HDM we refer the reader to [60]. By inspecting Eq. (29) it can be seen that $F_P \propto \frac{1}{2 \sin^2 \theta_W} \log \left(\frac{m_{H^\pm}^2}{m_t^2} \right)$ in the limit $m_{H^\pm} \rightarrow \infty$, hence recovering the result of the simplified model by identifying $\Lambda = m_{H^\pm}$. However, due to the unitarity bound the ratio m_{H^\pm}/m_t cannot be arbitrarily large, unless $\sin \theta \rightarrow 0$ so that the SM limit is properly recovered once $m_{H^\pm} \rightarrow \infty$. As a consequence one should consider a bound on $B_s \rightarrow \mu^+ \mu^-$ irrespective of the light pseudoscalar. By imposing that the NP contribution maintains the theoretical prediction for $B_s \rightarrow \mu^+ \mu^-$ within 3σ with respect to the experimental determination, one excludes values⁶ of $\tan \beta \lesssim 1$.

The bounds on $Br(B \rightarrow K \mu^+ \mu^-)$ can be derived analogously. The light pseudoscalar contribution to the effective action is determined by eq. 29. This contribution should be complemented by ones depending only on the heavy Higgs states as well as the SM contribution. The full expression of the branching ratio is rather complicated and we will not report it here explicitly and just refer to the literature [60, 62]. In order to keep the contributions from the heavy Higgses in agreement with observations, we will impose the bound $\tan \beta \gtrsim 2$ in the following.

The BaBar limits from the Υ decays are far simpler since this is a tree level process. It is sufficient to rescale $c_a^2 \rightarrow \sin^2 \theta \tan^2 \beta \frac{Br(a \rightarrow \mu^+ \mu^- (\tau^+ \tau^-))_{2\text{HDM}}}{Br(a \rightarrow \mu^+ \mu^- (\tau^+ \tau^-))_{\text{simplified}}}$, with $Br()_{2\text{HDM}}$ and $Br()_{\text{simplified}}$ being the decay branching ratio of a , in the indicated channels, in, respectively, the 2HDM+singlet model and in the simplified model studied in the previous section, and follow the procedure outlined in Sec. IC.

D. Results and Discussion

Similar to our discussion of the simplified model we compare the relative strength of the different constraints in the m_a - $\sin \theta$ plane for $m_\chi = 35$ GeV and $g_\chi = 0.5$. We need to keep in mind, however,

⁵ Our result disagrees with [48]. This is due to the fact that this reference relies on the computation performed in [79] which found that the branching ratio is enhanced by a factor $\tan \beta^4$. As pointed out by Refs. [62, 80], the result in [79] has been obtained by erroneously omitting relevant diagram and is gauge-dependent. The proper gauge invariant result does not exhibit a $\tan \beta$ enhancement.

⁶ This exclusion is approximately the same for all the 2HDM realizations with no flavor changing neutral currents induced a tree level. In the type-II model an additional excluded region appears for $\tan \beta \gtrsim 40$ and $m_{H^\pm} \lesssim 200$ GeV. We will not consider such low values of the mass in our analysis.

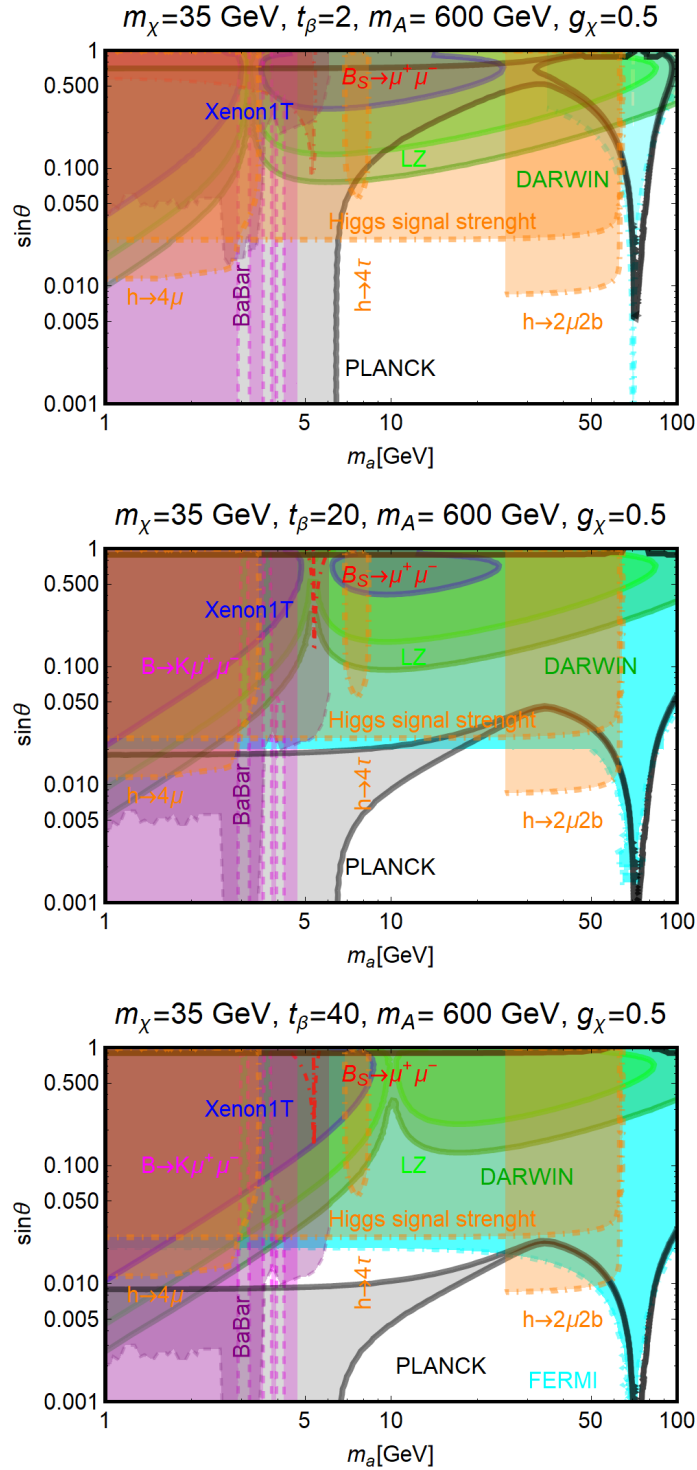
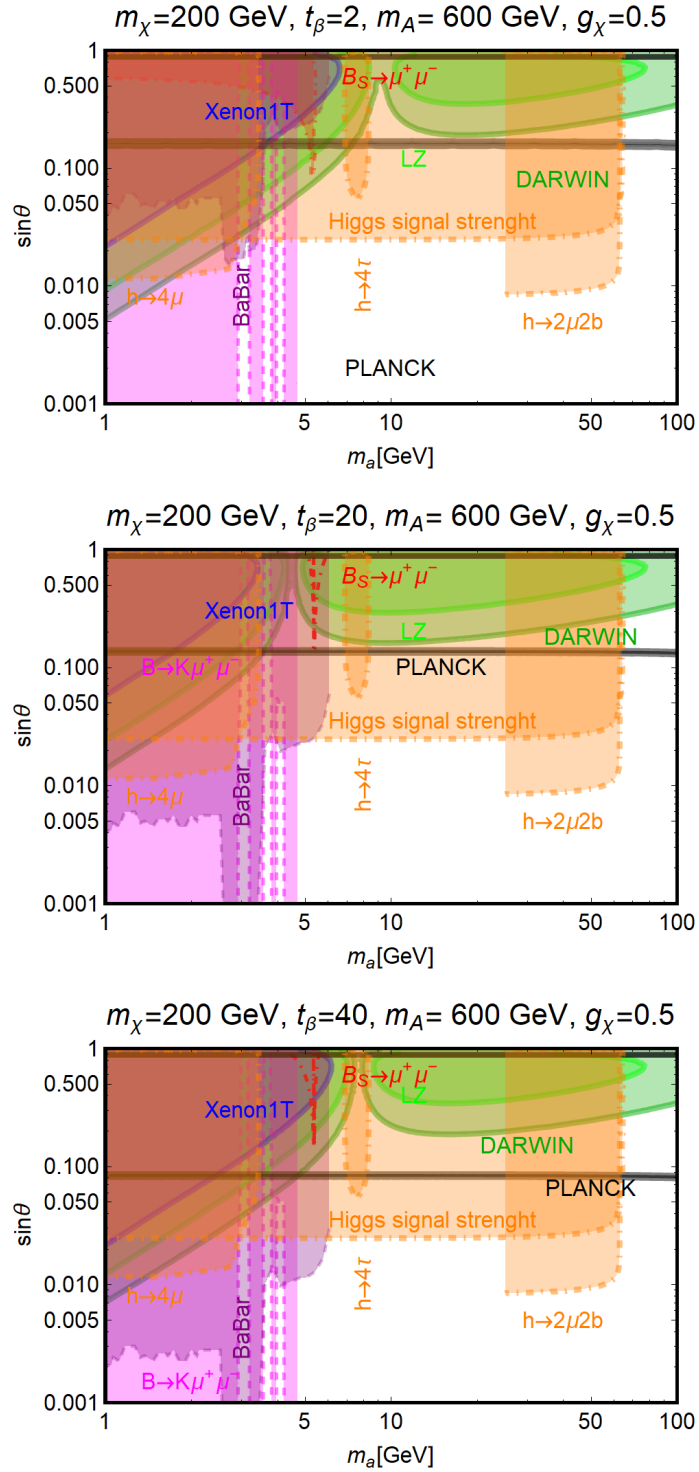


FIG. 6: Summary of constraints in the plane (m_a, θ) for fixed assignments of the other parameter, as reported on top of the panels. The correct DM relic density is achieved in the gray region labeled PLANCK. The blue region is excluded by XENON1T while the light (dark) green region shows the the projected sensitivity of LZ (DARWIN).

The cyan region labeled FERMI is excluded by indirect detection. In the red, magenta and purple region, one exceeds the experimental determination of $Br(B_s \rightarrow \mu^+ \mu^-)$ and $Br(B \rightarrow K \mu^+ \mu^-)$ and of the decay rate of Υ , respectively. The orange region is excluded by constraints from Higgs decays.

FIG. 7: Same as Fig. 6 for $m_\chi = 200$ GeV.

that the full model has additional parameters which can have an impact on the phenomenology. We set $m_A = m_H = m_{H^\pm} = 600$ GeV, close to the lower limit imposed by flavor observation and consider three different cases with $\tan\beta = 2, 20$ and 40 .

Again the gray regions highlight the part of the parameter space that produces the correct relic density. For the DM mass considered here, the main annihilation channels are still into aa and $\bar{b}b$ final states. The former mostly dominates at low values of m_a . Since for $\sin\theta \ll 1$ the corresponding rate is basically independent of the θ angle, the correct DM relic density is achieved in a broad region rather than along a narrow contour. At higher values of m_a , and in particular for $m_a > m_\chi$ the correct relic density is instead restricted to a narrow band and exhibits the expected pole at $m_\chi \sim \frac{m_a}{2}$ where the correct relic density is achieved for very low values of θ . Due to the $\tan\beta$ enhancement of the coupling of the pseudoscalar mediator with the b-quark the region of the correct relic density shifts towards lower values of θ as $\tan\beta$ increases.

Given that the DM annihilation cross section into $\bar{b}b$ final states is s-wave dominated this is accompanied by stronger limits from Fermi-LAT, see the cyan region in Fig. 6. Concerning direct detection, the limit/projected sensitivities only show a modest dependence on $\tan\beta$ but the shape of the curves exhibits some clear differences compared to the simplified scenario. This is due to the interplay between the two different contributions to the scalar effective operator. At low m_a the DM scattering cross section is dominated by the box-diagram while the triangle loop gives the largest contribution in the high m_a regime. At intermediate masses, a “blind spot” appears since the two contributions interfere destructively. At high values of $\tan\beta$, the region of the viable relic density moves increasingly away from the sensitivity of direct detection facilities. For $\tan\beta > 20$ only a small region, corresponding to light m_a masses, can be probed by DARWIN. This region is however completely ruled out by the constraints from $B \rightarrow K\mu^+\mu^-$. A further effective constraint is due to the $h \rightarrow aa$ decay. By considering only the bound from the Higgs signal strength, values of $\sin\theta$ greater than 0.05 are excluded within the full kinematical range of the $h \rightarrow aa$ decay, stronger bounds are obtained for more limited ranges of m_a when one considers searches of specific final states. Once this bound is enforced the correct DM relic density for $m_\chi = 35$ GeV can only be achieved in regions of parameter space that are out of reach of direct detection experiments. In summary, the case of $m_\chi = 35$ GeV appears to be very strongly constrained. Despite our revision, direct detection prospects remain irrelevant compared to bounds coming from low-energy/collider searches.

We consider a second benchmark with higher DM mass, namely $m_\chi = 200$ GeV. Despite the slightly lower sensitivity from direct detection experiments the high value of the DM mass has two advantages: the DM annihilation cross section is enhanced by the $\bar{t}t$, ha and Zh channels, so that the correct DM relic density can be achieved for higher values of m_a , to which flavor and collider bounds are not sensitive. Bounds from indirect detection are evaded since they cannot probe thermal DM with this such a high the mass yet. The results of our analysis is shown in Fig. 7. Contrary to the previous benchmark the relic density is constrained to two narrow lines. The line at $\sin\theta \simeq 1$ corresponds to a relic density mostly determined by annihilations into $\bar{t}t$ final states while at $\sin\theta \sim 0.1$ the dominant contribution is due to the ha final state. For $m_a > m_h/2$ the upper curve is unstrained by Higgs decay and can be tested by upcoming direct detection experiments.

Following the same procedure as in Sec. ID we select three benchmark points which are unconstrained by meson and Higgs decays, BM1 with ($m_a = 6$ GeV and $\sin\theta = 0.01$), BM2 with ($m_a = 50$ GeV and $\sin\theta = 0.005$) and BM3 with ($m_a = 100$ GeV and $\sin\theta = 0.1$). Each benchmark is considered for $\tan\beta = 2, 20$ and 40 while the mass of the heavy Higgses remains fixed at 600 GeV. We employ the relic density constraint to fix the value of g_χ as a function of m_χ and show the predicted values for $\sigma_{\chi p}^{SI}$ in Fig. 8. In contrast to the simplified model the expected scattering

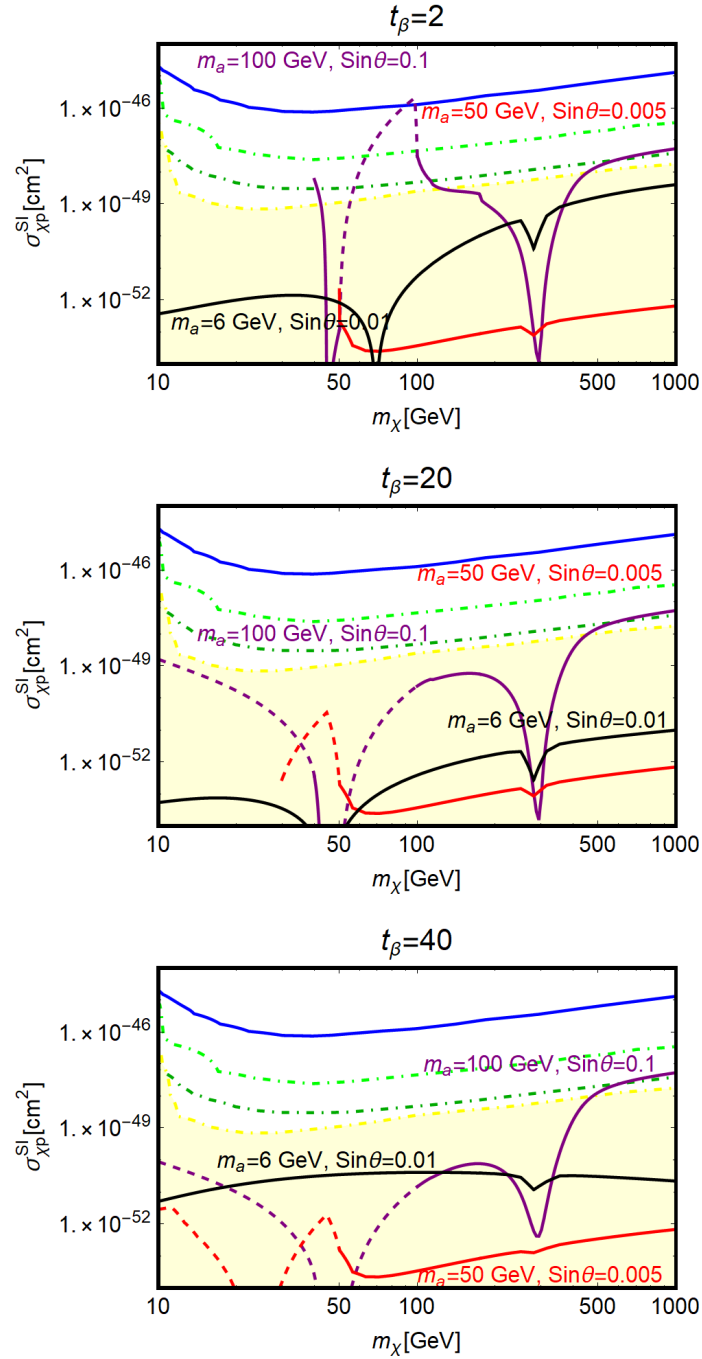


FIG. 8: Predictions for the direct detection cross section of thermal dark matter for three benchmark models with low $\tan\beta$, i.e. $t_\beta = 2$ (upper panel), medium $\tan\beta$, i.e. $t_\beta = 20$ (central panel), and high $\tan\beta$, i.e. $t_\beta = 40$ (lower panel). The solid parts of the lines are allowed by all other constraints while the dashed parts are excluded by indirect detection. In regions where the relic density can not be achieved with perturbative couplings the lines are discontinued. Also shown are the XENON1T limit (blue, solid), and the projected sensitivity of LZ (light green, dot-dashed) and DARWIN (dark green, dot-dashed). The yellow region is below the neutrino floor.

cross section of thermal dark matter is now a more complicated function of m_χ and the interplay of the box and the triangle contribution with the relic density constraint introduces a number of dips in $\sigma_{\chi p}^{SI}$. Nevertheless, it is clear that the scattering rate for light mediators is rather suppressed due to the strong bound on $\sin\theta$ from Higgs decays. For $m_a = 100$ GeV, on the other hand, detectable values $\sigma_{\chi p}^{SI}$ are still possible if either $\tan\beta$ is not too large or the annihilation rate is dominated by $t\bar{t}$ final states.

III. CONCLUSIONS

In this work, we have re-analyzed the direct detection prospects for dark matter models with pseudoscalar mediators. Since the tree-level dark matter-nucleon cross section is momentum suppressed the leading contribution to the direct detection rate arises at higher order. We have calculated the loop-induced contribution to the scattering rate in a simplified and in a more realistic, gauge-invariant model.

Using the relic density as our guiding principle and taking additional constraints from indirect detection and low energy observables into account we have identified the most promising regions for future direct detection experiments. In light of the constraints from meson decay, the detection of dark matter interacting via a very light pseudoscalar ($m_a \lesssim 5$ GeV) is challenging and can not be expected in the upcoming direct detection experiments. However, in the simplified model, we find promising regions of parameter space with $m_a = \mathcal{O}(10)$ GeV in which thermally produced dark matter can be tested by experiments with the sensitivity of the projected LZ and Darwin detectors. For heavier mediators, i.e. $m_a \sim 100$ GeV, an observation of dark matter-nucleon scattering might still be possible if the sensitivity can be pushed beyond the neutrino floor. At even higher masses collider searches can be expected to be the most restrictive experiments, again stressing the complementarity between direct detection and the LHC.

In order to assess whether these conclusions are robust, we repeat our analysis in a realistic completion of the simplified models. In the setup considered here, gauge invariance is restored by mixing the mediator with the pseudoscalar component of a 2HDM. Due to the larger scalar sector, additional interactions arise which change the global picture considerably. In particular, the new coupling between the pseudoscalar and the SM Higgs has an important impact on the phenomenology. On one hand, this coupling leads to decays of the SM-like Higgs h into pairs of pseudoscalars. The rate of such exotic Higgs decays is already tightly constrained by the observed Higgs signal strength and dedicated searches. In light of these limits, a detectable signal arising from the most promising parameter space identified in the simplified model, i.e. $m_a \approx 10$ GeV, is essentially ruled out. On the other hand, the same interaction also leads to an additional contribution to the direct detection rate which enhances the DD signal for heavier m_a relative to the simplified model. In particular, at high m_χ the predicted scattering rate is within reach of a Darwin-like device even for $m_a = 100$ GeV.

To conclude, we want to emphasize that despite their essentially vanishing dark matter-nucleon cross section at tree level, models with pseudoscalar mediators are potentially detectable with the next generation of direct detection experiments. In addition, they achieve such small scattering rates naturally, i.e. for $\mathcal{O}(1)$ couplings, and could, therefore, provide an important benchmark for upcoming direct dark matter searches. Finally, we would like to encourage the community to fully exploit the potential of direct detection experiments and think about new ways to extend the sensitivity beyond the neutrino floor.

Acknowledgments.— The authors thank L. Di Luzio and F. Mescia for the fruitful discussions. The authors also warmly thank D. McKeen and M. Freytsis for the kind exchange of correspondence. FSQ acknowledges support from MEC and ICTP-SAIFR FAPESP grant 2016/01343-7. WR is supported by the DFG with grant RO 2516/6-1 in the Heisenberg program.

Appendix A: SI Loop computation

In this appendix we sketch the derivation of the function F_l which determines the SI cross section, see Eq. 10. As already mentioned this scattering cross section is associated to the box diagram described in the Fig. 1. We have computed the diagram(s) with the package FeynCalc [81, 82], upon implementing the simplified model into FeynArts [83]. This computation allows to determine the following effective Lagrangian:

$$\begin{aligned}
\mathcal{L} = & A\bar{u}(p'_q)\gamma^\mu u(p_q)\bar{u}(p'_\chi)\gamma_\mu u(p_\chi) + B\bar{u}(p'_q)u(p_q)\bar{u}(p'_\chi)u(p_\chi) \\
& + \bar{u}(p'_q)\left(C_1\not{p}_\chi + C_2\not{p}'_\chi\right)u(p_q)\bar{u}(p'_\chi)u(p_\chi) + D\bar{u}(p'_q)\not{q}u(p_q)\bar{u}(p'_\chi)u(p_\chi) \\
& + E\bar{u}(p'_q)u(p_q)\bar{u}(p'_\chi)\not{p}'_q u(p_q) + \bar{u}(p'_q)\left(F_1\not{p}_\chi + F_2\not{p}'_\chi\right)u(p_q)\bar{u}(p'_\chi)\not{p}'_q u(p_\chi) \\
& + G\bar{u}(p'_q)\not{q}u(p_q)\bar{u}(p'_\chi)\not{p}'_q u(p_\chi)
\end{aligned} \tag{A1}$$

The operators containing $\not{q} = \not{p}_\chi - \not{p}'_\chi = \not{p}'_q - \not{p}_q$ become null once the Dirac equation is applied. By making repeated use of the equations of motion it is possible to reduce the effective Lagrangian (A1) to the sum of only one vectorial and one scalar operator, as written in (7), whose corresponding coefficients are given by (notice that C_1 and C_2 cancel each other one the external particles are put on shell):

$$\begin{aligned}
C_{V,q} &= A + m_q E + 2m_\chi m_q (F_1 + F_2) \\
C_{S,q} &= B
\end{aligned} \tag{A2}$$

Due to the Yukawa-like coupling structure vector interactions do not contribute to the scattering rate and we do not report them. The coefficient of the scalar coefficient can be evaluated analytically⁷

⁷ We use Package-X [84] for the reduction of the Passarino-Veltman functions.

and is given by

$$\begin{aligned}
C_{S,q} = & -\frac{1}{960\pi^2 m_q^3 m_\chi^3 m_a^4 (m_q - m_\chi)^3 (m_q + m_\chi)^3} \left[(m_q - m_\chi)^3 \left(m_q^4 m_a^4 (5m_\chi^2 (m_q + 3m_\chi) - m_a^2 (3m_q + 5m_\chi)) \log \left(\frac{m_\chi^2}{m_a^2} \right) \right. \right. \\
& - 2m_q^4 \sqrt{m_a^4 - 4m_\chi^2 m_a^2} (8m_q m_\chi^4 + m_\chi^2 m_a^2 (m_q - 5m_\chi) + m_a^4 (3m_q + 5m_\chi)) \log \left(\frac{\sqrt{m_a^4 - 4m_\chi^2 m_a^2} + m_a^2}{2m_\chi m_a} \right) \\
& + m_\chi^4 m_a^4 (5m_q^2 (3m_q + m_\chi) - m_a^2 (5m_q + 3m_\chi)) \log \left(\frac{m_q^2}{m_a^2} \right) \\
& + 2m_q^2 m_\chi^2 m_a^2 (m_q + m_\chi) (8m_q^2 m_\chi^2 - m_a^2 (3m_q^2 + 2m_q m_\chi + 3m_\chi^2)) \\
& - 2m_\chi^4 \sqrt{m_a^4 - 4m_q^2 m_a^2} (8m_q^4 m_\chi + m_q^2 m_a^2 (m_\chi - 5m_q) + m_a^4 (5m_q + 3m_\chi)) \log \left(\frac{\sqrt{m_a^4 - 4m_q^2 m_a^2} + m_a^2}{2m_q m_a} \right) \Big) \\
& + (m_q + m_\chi)^3 \left(m_q^4 m_a^4 (5m_\chi^2 (m_q - 3m_\chi) + m_a^2 (5m_\chi - 3m_q)) \log \left(\frac{m_\chi^2}{m_a^2} \right) \right. \\
& + 2m_q^4 \sqrt{m_a^4 - 4m_\chi^2 m_a^2} (-8m_q m_\chi^4 - m_\chi^2 m_a^2 (m_q + 5m_\chi) + m_a^4 (5m_\chi - 3m_q)) \log \left(\frac{\sqrt{m_a^4 - 4m_\chi^2 m_a^2} + m_a^2}{2m_\chi m_a} \right) \\
& + 2m_q^2 m_\chi^2 m_a^2 (m_q - m_\chi) (m_a^2 (-3m_q^2 + 2m_q m_\chi - 3m_\chi^2) + 8m_q^2 m_\chi^2) \\
& + 2m_\chi^4 \sqrt{m_a^4 - 4m_q^2 m_a^2} (8m_q^4 m_\chi + m_q^2 m_a^2 (5m_q + m_\chi) + m_a^4 (3m_\chi - 5m_q)) \log \left(\frac{\sqrt{m_a^4 - 4m_q^2 m_a^2} + m_a^2}{2m_q m_a} \right) \\
& \left. \left. + m_\chi^4 m_a^4 (15m_q^3 - 5m_q^2 m_\chi - 5m_q m_a^2 + 3m_\chi m_a^2) \log \left(\frac{m_q^2}{m_a^2} \right) \right] \right]. \tag{A3}
\end{aligned}$$

-
- [1] J. Silk *et al.*, *Particle Dark Matter: Observations, Models and Searches*. Cambridge Univ. Press, Cambridge, 2010.
- [2] **Planck** Collaboration, P. A. R. Ade *et al.*, *Planck 2015 results. XIII. Cosmological parameters*, *Astron. Astrophys.* **594** (2016) A13, [1502.01589].
- [3] G. Arcadi, M. Dutra, P. Ghosh, M. Lindner, Y. Mambrini, M. Pierre, S. Profumo, and F. S. Queiroz, *The Waning of the WIMP? A Review of Models, Searches, and Constraints*, 1703.07364.
- [4] **SuperCDMS** Collaboration, R. Agnese *et al.*, *Search for Low-Mass Weakly Interacting Massive Particles with SuperCDMS*, *Phys. Rev. Lett.* **112** (2014), no. 24 241302, [1402.7137].
- [5] **DarkSide** Collaboration, P. Agnes *et al.*, *Results from the first use of low radioactivity argon in a dark matter search*, *Phys. Rev.* **D93** (2016), no. 8 081101, [1510.00702]. [Addendum: Phys. Rev. D95, no. 6, 069901 (2017)].
- [6] **CRESST** Collaboration, G. Angloher *et al.*, *Results on light dark matter particles with a low-threshold CRESST-II detector*, *Eur. Phys. J.* **C76** (2016), no. 1 25, [1509.01515].
- [7] **LUX** Collaboration, D. S. Akerib *et al.*, *Results from a search for dark matter in the complete LUX exposure*, *Phys. Rev. Lett.* **118** (2017), no. 2 021303, [1608.07648].
- [8] **EDELWEISS** Collaboration, L. Hehn *et al.*, *Improved EDELWEISS-III sensitivity for low-mass WIMPs using a profile likelihood approach*, *Eur. Phys. J.* **C76** (2016), no. 10 548, [1607.03367].
- [9] T. Marrodn Undagoitia and L. Rauch, *Dark matter direct-detection experiments*, *J. Phys.* **G43** (2016), no. 1 013001, [1509.08767].

- [10] **PandaX-II** Collaboration, A. Tan *et. al.*, *Dark Matter Results from First 98.7 Days of Data from the PandaX-II Experiment*, *Phys. Rev. Lett.* **117** (2016), no. 12 121303, [1607.07400].
- [11] **PICO** Collaboration, C. Amole *et. al.*, *Dark Matter Search Results from the PICO-60 C₃F₈ Bubble Chamber*, *Phys. Rev. Lett.* **118** (2017), no. 25 251301, [1702.07666].
- [12] **XENON** Collaboration, E. Aprile *et. al.*, *First Dark Matter Search Results from the XENON1T Experiment*, 1705.06655.
- [13] **DEAP-3600** Collaboration, P. A. Amaudruz *et. al.*, *First results from the DEAP-3600 dark matter search with argon at SNOLAB*, 1707.08042.
- [14] M. Duerr, F. Kahlhoefer, K. Schmidt-Hoberg, T. Schwetz, and S. Vogl, *How to save the WIMP: global analysis of a dark matter model with two s-channel mediators*, *JHEP* **09** (2016) 042, [1606.07609].
- [15] G. Arcadi, C. Gross, O. Lebedev, S. Pokorski, and T. Toma, *Evading Direct Dark Matter Detection in Higgs Portal Models*, *Phys. Lett.* **B769** (2017) 129–133, [1611.09675].
- [16] G. Arcadi, F. S. Queiroz, and C. Siqueira, *The Semi-Hooperon: Gamma-ray and anti-proton excesses in the Galactic Center*, 1706.02336.
- [17] A. Berlin, D. Hooper, and S. D. McDermott, *Simplified Dark Matter Models for the Galactic Center Gamma-Ray Excess*, *Phys. Rev.* **D89** (2014), no. 11 115022, [1404.0022].
- [18] C. Arina, E. Del Nobile, and P. Panci, *Dark Matter with Pseudoscalar-Mediated Interactions Explains the DAMA Signal and the Galactic Center Excess*, *Phys. Rev. Lett.* **114** (2015) 011301, [1406.5542].
- [19] M. J. Dolan, F. Kahlhoefer, C. McCabe, and K. Schmidt-Hoberg, *A taste of dark matter: Flavour constraints on pseudoscalar mediators*, *JHEP* **03** (2015) 171, [1412.5174]. [Erratum: *JHEP*07,103(2015)].
- [20] J. M. No, *Looking through the pseudoscalar portal into dark matter: Novel mono-Higgs and mono-Z signatures at the LHC*, *Phys. Rev.* **D93** (2016), no. 3 031701, [1509.01110].
- [21] X. Liu, L. Bian, X.-Q. Li, and J. Shu, *Type-III two Higgs doublet model plus a pseudoscalar confronted with $h \rightarrow \mu\tau$, muon $g - 2$ and dark matter*, *Nucl. Phys.* **B909** (2016) 507–524, [1508.05716].
- [22] J. Fan, S. M. Koushiappas, and G. Landsberg, *Pseudoscalar Portal Dark Matter and New Signatures of Vector-like Fermions*, *JHEP* **01** (2016) 111, [1507.06993].
- [23] O. Buchmueller, S. A. Malik, C. McCabe, and B. Penning, *Constraining Dark Matter Interactions with Pseudoscalar and Scalar Mediators Using Collider Searches for Multijets plus Missing Transverse Energy*, *Phys. Rev. Lett.* **115** (2015), no. 18 181802, [1505.07826].
- [24] A. Berlin, S. Gori, T. Lin, and L.-T. Wang, *Pseudoscalar Portal Dark Matter*, *Phys. Rev.* **D92** (2015) 015005, [1502.06000].
- [25] S. Banerjee, D. Barducci, G. Blanger, B. Fuks, A. Goudelis, and B. Zaldivar, *Cornering pseudoscalar-mediated dark matter with the LHC and cosmology*, *JHEP* **07** (2017) 080, [1705.02327].
- [26] M. Bauer, U. Haisch, and F. Kahlhoefer, *Simplified dark matter models with two Higgs doublets: I. Pseudoscalar mediators*, *JHEP* **05** (2017) 138, [1701.07427].
- [27] S. Baek, P. Ko, and J. Li, *Minimal renormalizable simplified dark matter model with a pseudoscalar mediator*, *Phys. Rev.* **D95** (2017), no. 7 075011, [1701.04131].
- [28] M. Freytsis and Z. Ligeti, *On dark matter models with uniquely spin-dependent detection possibilities*, *Phys. Rev.* **D83** (2011) 115009, [1012.5317].
- [29] C. Boehm, M. J. Dolan, C. McCabe, M. Spannowsky, and C. J. Wallace, *Extended gamma-ray emission from Coy Dark Matter*, *JCAP* **1405** (2014) 009, [1401.6458].
- [30] K.-C. Yang, *Fermionic Dark Matter through a Light Pseudoscalar Portal: Hints from the DAMA Results*, *Phys. Rev.* **D94** (2016), no. 3 035028, [1604.04979].
- [31] J. Billard, L. Strigari, and E. Figueroa-Feliciano, *Implication of neutrino backgrounds on the reach of next generation dark matter direct detection experiments*, *Phys. Rev.* **D89** (2014), no. 2 023524, [1307.5458].
- [32] F. Ruppin, J. Billard, E. Figueroa-Feliciano, and L. Strigari, *Complementarity of dark matter detectors in light of the neutrino background*, *Phys. Rev.* **D90** (2014), no. 8 083510, [1408.3581].
- [33] J. H. Davis, *Dark Matter vs. Neutrinos: The effect of astrophysical uncertainties and timing information on the neutrino floor*, *JCAP* **1503** (2015) 012, [1412.1475].
- [34] B. Dutta, R. Mahapatra, L. E. Strigari, and J. W. Walker, *Sensitivity to Z-prime and nonstandard neutrino interactions from ultralow threshold neutrino-nucleus coherent scattering*, *Phys. Rev.* **D93**

- (2016), no. 1 013015, [1508.07981].
- [35] J. B. Dent, B. Dutta, J. L. Newstead, and L. E. Strigari, *Effective field theory treatment of the neutrino background in direct dark matter detection experiments*, *Phys. Rev.* **D93** (2016), no. 7 075018, [1602.05300].
- [36] K. C. Y. Ng, J. F. Beacom, A. H. G. Peter, and C. Rott, *Solar Atmospheric Neutrinos: A New Neutrino Floor for Dark Matter Searches*, 1703.10280.
- [37] **XENON** Collaboration, E. Aprile *et. al.*, *Physics reach of the XENON1T dark matter experiment*, *JCAP* **1604** (2016), no. 04 027, [1512.07501].
- [38] **LUX, LZ** Collaboration, M. Szydagis, *The Present and Future of Searching for Dark Matter with LUX and LZ*, *PoS ICHEP2016* (2016) 220, [1611.05525].
- [39] **DARWIN** Collaboration, J. Aalbers *et. al.*, *DARWIN: towards the ultimate dark matter detector*, *JCAP* **1611** (2016) 017, [1606.07001].
- [40] D. Goncalves, P. A. N. Machado, and J. M. No, *Simplified Models for Dark Matter Face their Consistent Completions*, *Phys. Rev.* **D95** (2017), no. 5 055027, [1611.04593].
- [41] M. R. Buckley, D. Feld, and D. Goncalves, *Scalar Simplified Models for Dark Matter*, *Phys. Rev.* **D91** (2015) 015017, [1410.6497].
- [42] P. Harris, V. V. Khoze, M. Spannowsky, and C. Williams, *Constraining Dark Sectors at Colliders: Beyond the Effective Theory Approach*, *Phys. Rev.* **D91** (2015) 055009, [1411.0535].
- [43] P. Gondolo and G. Gelmini, *Cosmic abundances of stable particles: Improved analysis*, *Nucl. Phys.* **B360** (1991) 145–179.
- [44] D. Barducci, G. Belanger, J. Bernon, F. Boudjema, J. Da Silva, S. Kraml, U. Laa, and A. Pukhov, *Collider limits on new physics within micrOMEGAs4.3*, 1606.03834.
- [45] **Fermi-LAT** Collaboration, M. Ackermann *et. al.*, *Searching for Dark Matter Annihilation from Milky Way Dwarf Spheroidal Galaxies with Six Years of Fermi Large Area Telescope Data*, *Phys. Rev. Lett.* **115** (2015), no. 23 231301, [1503.02641].
- [46] **Fermi-LAT** Collaboration, M. Ackermann *et. al.*, *Updated search for spectral lines from Galactic dark matter interactions with pass 8 data from the Fermi Large Area Telescope*, *Phys. Rev.* **D91** (2015) 122002, [1506.00013].
- [47] **Cherenkov Telescope Array Consortium** Collaboration, B. S. Acharya *et. al.*, *Science with the Cherenkov Telescope Array*, 1709.07997.
- [48] S. Ipek, D. McKeen, and A. E. Nelson, *A Renormalizable Model for the Galactic Center Gamma Ray Excess from Dark Matter Annihilation*, *Phys. Rev.* **D90** (2014) 055021, [1404.3716].
- [49] M. Drees and M. Nojiri, *Neutralino - nucleon scattering revisited*, *Phys. Rev.* **D48** (1993) 3483–3501, [hep-ph/9307208].
- [50] M. A. Shifman, A. I. Vainshtein, and V. I. Zakharov, *Remarks on Higgs Boson Interactions with Nucleons*, *Phys. Lett.* **78B** (1978) 443–446.
- [51] J. R. Ellis, K. A. Olive, and C. Savage, *Hadronic Uncertainties in the Elastic Scattering of Supersymmetric Dark Matter*, *Phys. Rev.* **D77** (2008) 065026, [0801.3656].
- [52] J. Hisano, K. Ishiwata, and N. Nagata, *Gluon contribution to the dark matter direct detection*, *Phys. Rev.* **D82** (2010) 115007, [1007.2601].
- [53] P. Fayet, *U-boson production in e^+e^- annihilations, ψ and Upsilon decays, and Light Dark Matter*, *Phys. Rev.* **D75** (2007) 115017, [hep-ph/0702176].
- [54] S. Andreas, O. Lebedev, S. Ramos-Sanchez, and A. Ringwald, *Constraints on a very light CP-odd Higgs of the NMSSM and other axion-like particles*, *JHEP* **08** (2010) 003, [1005.3978].
- [55] **BaBar** Collaboration, J. P. Lees *et. al.*, *Search for hadronic decays of a light Higgs boson in the radiative decay $\Upsilon \rightarrow \gamma A^0$* , *Phys. Rev. Lett.* **107** (2011) 221803, [1108.3549].
- [56] **BaBar** Collaboration, J. P. Lees *et. al.*, *Search for di-muon decays of a low-mass Higgs boson in radiative decays of the $(1S)$* , *Phys. Rev.* **D87** (2013), no. 3 031102, [1210.0287]. [Erratum: *Phys. Rev.* **D87**, no. 5, 059903(2013)].
- [57] **BaBar** Collaboration, J. P. Lees *et. al.*, *Search for a low-mass scalar Higgs boson decaying to a tau pair in single-photon decays of $\Upsilon(1S)$* , *Phys. Rev.* **D88** (2013), no. 7 071102, [1210.5669].
- [58] **LHCb, CMS** Collaboration, V. Khachatryan *et. al.*, *Observation of the rare $B_s^0 \rightarrow \mu^+ \mu^-$ decay from the combined analysis of CMS and LHCb data*, *Nature* **522** (2015) 68–72, [1411.4413].

- [59] **LHCb** Collaboration, R. Aaij *et. al.*, *Precision measurement of CP violation in $B_s^0 \rightarrow J/\psi K^+ K^-$ decays*, *Phys. Rev. Lett.* **114** (2015), no. 4 041801, [1411.3104].
- [60] P. Arnan, D. Beirevi, F. Mescia, and O. Sumensari, *Two Higgs Doublet Models and $b \rightarrow s$ exclusive decays*, 1703.03426.
- [61] W. Altmannshofer, P. Paradisi, and D. M. Straub, *Model-Independent Constraints on New Physics in $b \rightarrow s$ Transitions*, *JHEP* **04** (2012) 008, [1111.1257].
- [62] X.-Q. Li, J. Lu, and A. Pich, *$B_{s,d}^0 \rightarrow \ell^+ \ell^-$ Decays in Two-Higgs Doublet Models*, *Nucl. Part. Phys. Proc.* **273-275** (2016) 1411–1416, [1410.4775].
- [63] **HPQCD** Collaboration, C. Bouchard, G. P. Lepage, C. Monahan, H. Na, and J. Shigemitsu, *Rare decay $B \rightarrow K \ell^+ \ell^-$ form factors from lattice QCD*, *Phys. Rev.* **D88** (2013), no. 5 054509, [1306.2384]. [Erratum: *Phys. Rev.* **D88**, no. 7, 079901 (2013)].
- [64] V. Baru, E. Epelbaum, A. A. Filin, J. Gegelia, and A. V. Nefediev, *Binding energy of the $X(3872)$ at unphysical pion masses*, *Phys. Rev.* **D92** (2015), no. 11 114016, [1509.01789].
- [65] **LHCb** Collaboration, R. Aaij *et. al.*, *Differential branching fraction and angular analysis of the $B^+ \rightarrow K^+ \mu^+ \mu^-$ decay*, *JHEP* **02** (2013) 105, [1209.4284].
- [66] A. X. Gonzalez-Morales, S. Profumo, and F. S. Queiroz, *Effect of Black Holes in Local Dwarf Spheroidal Galaxies on Gamma-Ray Constraints on Dark Matter Annihilation*, *Phys. Rev.* **D90** (2014), no. 10 103508, [1406.2424].
- [67] P. Tunney, J. M. No, and M. Fairbairn, *A Novel LHC Dark Matter Search to Dissect the Galactic Centre Excess*, 1705.09670.
- [68] N. F. Bell, G. Busoni, and I. W. Sanderson, *Self-consistent Dark Matter Simplified Models with an s-channel scalar mediator*, *JCAP* **1703** (2017), no. 03 015, [1612.03475].
- [69] N. F. Bell, G. Busoni, and I. W. Sanderson, *Two Higgs Doublet Dark Matter Portal*, 1710.10764.
- [70] G. C. Branco, P. M. Ferreira, L. Lavoura, M. N. Rebelo, M. Sher, and J. P. Silva, *Theory and phenomenology of two-Higgs-doublet models*, *Phys. Rept.* **516** (2012) 1–102, [1106.0034].
- [71] **CMS** Collaboration, V. Khachatryan *et. al.*, *Search for resonant $t\bar{t}$ production in proton-proton collisions at $\sqrt{s} = 8\text{TeV}$* , *Phys. Rev.* **D93** (2016), no. 1 012001, [1506.03062].
- [72] **ATLAS** Collaboration, G. Aad *et. al.*, *A search for $t\bar{t}$ resonances using lepton-plus-jets events in proton-proton collisions at $\sqrt{s} = 8\text{ TeV}$ with the ATLAS detector*, *JHEP* **08** (2015) 148, [1505.07018].
- [73] **ATLAS** Collaboration, G. Aad *et. al.*, *Search for neutral Higgs bosons of the minimal supersymmetric standard model in pp collisions at $\sqrt{s} = 8\text{ TeV}$ with the ATLAS detector*, *JHEP* **11** (2014) 056, [1409.6064].
- [74] **CMS** Collaboration, V. Khachatryan *et. al.*, *Search for neutral MSSM Higgs bosons decaying to a pair of tau leptons in pp collisions*, *JHEP* **10** (2014) 160, [1408.3316].
- [75] M. Baak, M. Goebel, J. Haller, A. Hoecker, D. Ludwig, K. Moenig, M. Schott, and J. Stelzer, *Updated Status of the Global Electroweak Fit and Constraints on New Physics*, *Eur. Phys. J.* **C72** (2012) 2003, [1107.0975].
- [76] M. Misiak and M. Steinhauser, *Weak radiative decays of the B meson and bounds on M_{H^\pm} in the Two-Higgs-Doublet Model*, *Eur. Phys. J.* **C77** (2017), no. 3 201, [1702.04571].
- [77] **CMS** Collaboration, V. Khachatryan *et. al.*, *Search for light bosons in decays of the 125 GeV Higgs boson in proton-proton collisions at $\sqrt{s} = 8\text{ TeV}$* , 1701.02032.
- [78] *Measurements of the Higgs boson production and decay rates and constraints on its couplings from a combined ATLAS and CMS analysis of the LHC pp collision data at $\sqrt{s} = 7$ and 8 TeV*, Tech. Rep. ATLAS-CONF-2015-044, CERN, Geneva, Sep, 2015.
- [79] W. Skiba and J. Kalinowski, *$B_s \rightarrow \tau^+ \tau^-$ decay in a two Higgs doublet model*, *Nucl. Phys.* **B404** (1993) 3–19.
- [80] H. E. Logan and U. Nierste, *$B_{s,d} \rightarrow \ell^+ \ell^-$ in a two Higgs doublet model*, *Nucl. Phys.* **B586** (2000) 39–55, [hep-ph/0004139].
- [81] R. Mertig, M. Bohm, and A. Denner, *FEYN CALC: Computer algebraic calculation of Feynman amplitudes*, *Comput. Phys. Commun.* **64** (1991) 345–359.
- [82] V. Shtabovenko, R. Mertig, and F. Orellana, *New Developments in FeynCalc 9.0*, *Comput. Phys. Commun.* **207** (2016) 432–444, [1601.01167].

- [83] T. Hahn, *Generating Feynman diagrams and amplitudes with FeynArts 3*, *Comput. Phys. Commun.* **140** (2001) 418–431, [[hep-ph/0012260](#)].
- [84] H. H. Patel, *Package-X: A Mathematica package for the analytic calculation of one-loop integrals*, *Comput. Phys. Commun.* **197** (2015) 276–290, [[1503.01469](#)].